IOP Publishing Measurement Science and Technology
Meas. Sci. Technol. **33** (2022) 095103 (14pp) https://doi.org/10.1088/1361-6501/ac7435

# Variation of receiver code biases under the influence of the receiver type and antenna configuration in the IGS network

**Luohong Li**[1,2], **Xinyu Zhang**[1,2] **and Yunbin Yuan**[1,*]

[1] State Key Laboratory of Geodesy and Earth's Dynamics, Innovation Academy for Precision Measurement Science and Technology, Chinese Academy of Sciences, Wuhan, People's Republic of China
[2] College of Earth and Planetary Sciences, University of Chinese Academy of Sciences, Beijing, People's Republic of China

E-mail: yybgps@whigg.ac.cn

Received 25 January 2022, revised 12 May 2022
Accepted for publication 27 May 2022
Published 9 June 2022

**Abstract**

Receiver code biases (RCBs) are known to be time delays within the receiver caused by their hardware imperfections. To better understand the characteristics of RCBs, the un-combined (UC) and ionosphere-free (IF) precise point positioning functional models are adapted and re-parameterized to estimate the variation of RCBs as a time-variant parameter. In this study, we analytically studied the temporal variations of RCBs; although there exists a benchmark difference between the UC and IF models, their estimates are in accordance with each other. Additionally, this contribution assesses the inter-day stability of RCBs with weekly observations from 165 globally distributed international global navigation satellite system service stations equipped the receivers of three mainly types. The inter-day stability results of RCB revealed that the RCBs of POL2 and OUS2 have better stability over consecutive 7 d and the single differenced (SD) RCBs can reach 0.2 m in the best case. The results show that 74.83% of the stations are equipped with Trimble receivers under the condition that the mean SD RCB values are between −0.5 and 0.5 m, while 85.57% of the stations are equipped with Septentrio receivers and the stations equipped with Javad can reach 84.35% under this condition. The RCB estimates are also relatively stable for the case in which the receiver hardware device stays unchanged. The relationship between RCBs, receiver type, and antenna configuration is found using six groups of receivers. A strong correlation exists between RCBs, receiver type, and antenna configuration, which is more obvious among Septentrio receivers. The results show that the Pearson correlation coefficients were all higher than 0.9, and the standard deviation of between-receiver RCBs was smaller than 0.327 m when equipped with Septentrio receivers. We concluded that there is a strong relationship between the receiver-related pseudorange biases and the receiver and antenna setup.

Keywords: receiver code biases (RCB), global positioning system (GPS), functional model

(Some figures may appear in color only in the online journal)

* Author to whom any correspondence should be addressed.

 

## 1. Introduction

Code biases from the global navigation satellite systems (GNSSs) are known to be time delays within the satellite and receiver caused by their hardware imperfections. This delay has to be considered when processing GNSS data for several applications, such as satellite and receiver clock estimation, ambiguity resolution (AR) in the phase observation, and ionosphere analysis [1, 2]. There is a general demand for better positioning accuracy and faster position acquisition from both the users and the GNSS research community. Hence, accounting for the biases in the positioning model is a prerequisite for a stronger positioning model and ensures better performance of the high-precision positioning system and accurate results with precise point positing (PPP) [3, 4].

According to previous studies, multiple bias items have been proposed and estimated in the GNSS pseudorange observations [5–7], which are used to separate the biases from the observations and improve the accuracy of observation data. With the rapid development of multi-GNSS, it provides us a good opportunity to monitor and study ionosphere with multi-GNSS and multi frequency observation data. Thus, the multi types of differential code biases (DCBs) are formed based on the multi-GNSS and multi frequency GNSS observations. This code bias is considered to consist of two components: the satellite-dependent and receiver-dependent biases. The satellite-dependent part is usually attributed to the satellite hardware end, namely, the satellite code biases (SCBs), which exist on each pseudorange signal that the satellite transmits. The absolute form of SCBs is hard to calculate, and we adapt the differenced form of SCBs, which is defined as the difference between two signals with different frequencies. The DCB has already been studied in previous work, and it needs to be carefully calibrated when sensing the ionosphere through GNSS [8, 9]. The SCB can be corrected as a constant with the corresponding multi-GNSS DCB products, which are routinely provided by the German Aerospace Center (DLR) and the Chinese Academy of Sciences (CAS). Moreover, the satellite DCBs can be estimated as constants over one day with relatively high accuracy (as good as 0.1 ns) and high-level stability (as good as 0.2 ns). Their impact on the modeling of the ionospheric total electron content (TEC) can be easily removed [10]. However, owing to a growing variety of GNSS signals and observables, the DCB corrections are unsuitable and inconvenient to be extended to multi-GNSS and multi-frequency observations. Compared to a relative form of bias using DCB corrections, the pseudo-absolute code biases provided in observable-specific signal bias (OSB) products is an approach towards a flexible, expandable handling of GNSS bias [11, 12]. In addition to temporal scale variation of SCBs, Li *et al* [13] estimate GNSS DCBs with the onboard receiver of the China Fengyun-3C satellite. The results indicate that the onboard receiver DCB is very stable. Therefore, the SCBs have been handled effectively with the current method and products. Besides, there are also different biases related to frequency and receiver proposed in recently years, such as inter system bias (ISB), inter frequency bias and un-calibrated phase delay. Liu *et al* [14] set up the ISB parameters for GLONASS, BDS, and Galileo as 1 d constants to assess the positioning performance of multi-GNSS PPP. Khodabandeh and Teunissen [15] proposed to generate an ISB look-up table to allow users to search the table for a network receiver of their own type and select the corresponding ISBs in PPP-real-time kinematic (RTK). Jiang *et al* [16] estimated the ISBs as piece-wise constant every 30 min and developed a short-term station-dependent ISB prediction model. However, the mechanisms of those biases are obscure, which is an obstacle in multi-GNSS PPP processing due to a lack of accurate GNSS correction information. The satellite-induced pseudo-range multi-path error that elevation angle related in BeiDou system (BDS-2) has been investigated in great details and has been modeled by Wanninger and Beer [17] for non geostationary earth orbit satellites. Although there are so many types of biases found and modeled, the comprehensive evaluation and modeling of the biases is a difficult and frontal subject.

The topic of GNSS receiver code biases (RCBs) has garnered considerable attention in recent years [18–21]. The introduction of biases requires knowledge of biases in the receiver hardware that tend to be specific to the receiver model. Similar to the characteristics of the SCB, the biases are a result of small delays, between events that ideally should be simultaneous, in the reception of the signal in a GNSS receiver. The existence of receiver-specific code bias has a few adverse impacts, including the loss of position accuracy in single point positioning, delay of the PPP convergence performance, obstruction of PPP AR, reduction of the RTK ratio and the RTK fixing rate, and the loss of precision of DCB estimates [22–24]. This further increases the need for understanding GNSS receiver hardware biases, as it can facilitate both an increase in the accuracy of the positioning solution and a reduction in the solution convergence time.

Recently, the issues of RCB, like its origin and property, have been of substantial concern. Moreover, a functional model has been established to proceed with the PPP, which is subject to extensive research [25–27]. Improper estimation of the receiver-specific code biases blocks the convergence performance of PPP and postpones its AR when using GNSS measurements of mixed receiver types [28]. Based on the assumption that code biases could be treated as a constant in the short term [29], RCBs are re-estimated every 24 h for convenience. Lately, an increasing number of experimental results point to the intra-day variation of RCBs [30, 31], which is inconsistent with the former assumption. The magnitude of the receiver code is closely related to the receiver equipment, such as the receiver type, the antenna type, and the firmware version [32, 33]. Gong *et al* [18] found that considering time-variant RCBs can accelerate the convergence of the PPP model. Furthermore, Zha *et al* [34] found that the variability of RCBs are closely associated with the firmware updates and temperature variations of the receiver, and they may demonstrate significant variations over a time period of 1 d or even a few hours, which have been observed as DCB estimates in different studies. Additionally, the magnitude of the variation within a receiver DCB corresponding to one of the short-baselines can exceed 6.5 ns (1.8 m) over the course of 1 d [35]. The difference in RCBs may be related to the different types of

receivers [19, 22]. Therefore, the modification of the original PPP model is a crucial requisite to reduce negative influences by time-variant code biases.

The code biases are hard to estimate in their undifferenced form, as they are highly correlated with other terms, such as clock errors. We modified the functional model of PPP with re-parameterization and S-transformations, as required. As for the PPP model and its variants, Zhang *et al* [36] established a modified PPP (MPPP) full-rank model using the receiver-specific code bias as a variate and estimating it in every epoch. They found that the receiver-specific code bias varied exactly in the range of 10 ns in a certain period of time. Moreover, the MPPP model enhances the AR capability, accelerates the convergence of positioning results, and reduces leveling errors in the slant total electron content estimation. The MPPP model is stable in determining the variation of receiver-specific code biases, which is useful in reducing the loss of positional accuracy and provides a platform for analyzing the properties of RCBs. Nevertheless, there are limited studies to discuss the relationship between RCBs and the receiver type and antenna configuration [37], although RCBs are caused by their hardware imperfections. Besides, although many studies have proved the equivalence of un-combined (UC) PPP and ionosphere-free (IF) PPP [38], the MPPP model is proposed with UC observables, and a modified functional model with IF observables should also be followed up and be focused on. With the modified functional model that can accurately capture the variation of RCBs, we can explore the behavior of RCBs under the influence of hardware and study its character, which is important and significant for GNSS data processing with data from mixed-receiver.

The organization of this work proceeds as follows. In section 2, we first discuss the raw observations, and then present two MPPP full-rank functional models by re-parameterization: IF and UC PPP models, followed by the interpretation of the treatment of rank deficiency. Section 3 presents the results of the temporal variations of the RCBs, the inter-day stability of RCBs, and characteristics related to the receiver type and antenna configuration. Finally, the conclusions of this study are provided in section 4.

## 2. Methods

As mentioned above, the neglection of RCBs in the GNSS PPP model will change the vital parameters, including receiver clock and carrier phase ambiguities, even in the ionosphere. Therefore, the MPPP functional model was proposed to sensitively capture the time-variant characteristics of code biases. This section outlines the procedure of our time-wise retrieval approach of RCBs. We briefly illustrate two functional models that are adopted to obtain time-variant RCB estimates and the consistency between IF- and UC-derived estimates.

### 2.1. Raw GNSS observation equations

In GNSS data processing, considering time-variant and time-invariant code biases, the raw pseudorange and phase observation are defined as follows [39]:

$$\begin{cases} p^s_{r,j}(i) = \rho^s_r(i) + dt_r(i) - dt^s(i) + m^s_r T^s_r(i) + \mu_j I^s_r(i) + b_{r,j}(i) - b^s_j + e^s_{r,j} \\ \phi^s_{r,j}(i) = \rho^s_r(i) + dt_r(i) - dt^s(i) + m^s_r T^s_r(i) - \mu_j I^s_r(i) + \lambda_j N^s_{r,j} + \varepsilon^s_{r,j} \end{cases} \tag{1}$$

where $r$, $s$, $j$ and $i$ represent the receiver, satellite, frequency, and epoch indices, respectively; where $p^s_{r,j}$ and $\phi^s_{r,j}$ denote, the code and phase observables, respectively; $\rho^s_r$ is the receiver-satellite range; $T^s_{r,j}$ denotes the troposphere delay, which can be converted to slant delay using the corresponding troposphere mapping function $m^s_r$; $dt_r$ and $dt^s$ denote the receiver and satellite clock offsets, respectively; $b_{r,j}$ and $b^s_j$ are the frequency-dependent receiver-specific and satellite-specific code biases, respectively; $\lambda_j$ is the wavelength of the phase measurement on the frequency band $j$; $I^s_r$ is the (first-order) slant ionosphere delay on the first frequency band; $\mu_j$ is the frequency-dependent multiplier factor at frequency $j$, which can be expressed as $\mu_j = \lambda_j^2/\lambda_1^2$; $N^s_{r,j}$ represents the (non-integer) ambiguity of each frequency (cycle); $e^s_{r,j}$ and $\varepsilon^s_{r,j}$ are the sums of noise and multipath error for the code and carrier phase observations, respectively. Notably, all quantities are within a unit of range except for $N^s_{r,j}$, and the time-constant parameters do not have an epoch index $i$. Notably, the receiver-specific biases are considered to be a time-variant parameter, while satellite-specific code biases are regarded as a constant that can be corrected by the products. Thus, the form of the receiver-specific biases is defined as $b_{r,j}(i)$ for an epoch-wise parameter.

The Kalman filter is used in the parameter estimation model, which necessitates that the above observation equations be linearized. The linearized form of equation (1) is as follows:

$$\begin{cases} \Delta p^s_{r,j}(i) = dt_r(i) + m^s_r Z_r(i) + \mu_j I^s_r(i) + b_{r,j}(i) + b^s_j + e^s_{r,j} + b^s_{\mathrm{IF}} \\ \Delta \phi^s_{r,j}(i) = dt_r(i) + m^s_r Z_r(i) - \mu_j I^s_r(i) + \lambda_j N^s_{r,j} + \varepsilon^s_{r,j} + b^s_{\mathrm{IF}} \end{cases} \tag{2}$$

where $p^s_{r,j}(i)$ and $\Delta\phi^s_{r,j}(i)$ denote the observed-minus-calculated pseudorange and carrier phase observation, respectively, which are corrected for the approximate receiver-satellite ranges and the satellite clocks. $m^s_r$ denotes the tropospheric wet mapping function. $Z_r(i)$ denotes the tropospheric zenith wet delay when the tropospheric zenith hydrostatic delay was corrected by the model. The receiver coordinates are fixed to the values in the international GNSS service (IGS) solution independent exchange (SINEX) product and are not part of the estimation parameters. If the receiver position is further regarded as an unknown, the derived model will not change. The satellite positions and clocks are computed with the Wuhan University Multi-GNSS final precise products (WUM). Conventionally, the precise satellite clock products estimated using IF observations are biased by the IF combination of the satellite instrument's time-invariant code delay $d\bar{t}^s = dt^s + b^s_{\mathrm{IF}}$ [40]. Therefore, after using the precise satellite clock products, the satellite clock parameter can be removed; however, the satellite-specific pseudorange biases $b^s_{\mathrm{IF}}$ are retained in the equation and will be effectively handled subsequently. Notably, the satellite and receiver antenna phase center offsets (PCOs) and phase center variations, relativistic effects, tidal loadings, and phase wind-up (only for the carrier phase) have been corrected with the existing models.

In this paper, to derive the accurate receiver-specific pseudorange biases, the IF and UC PPP models are both adopted. Notably, only the dual-frequency case is discussed to clearly show the functional model in a simple manner.

### 2.2. Ionosphere-free (IF) PPP model

When IF observations are constructed using GNSS dual-frequency measurements, the first-order ionospheric delay can be eliminated, and the corresponding equations and stochastic model are as follows:

$$\begin{cases} \Delta p^s_{r,\mathrm{IF}}(i) = d\tilde{t}_r(i) + m^s_r Z_r(i) + \tilde{b}_{r,\mathrm{IF}}(i) + e^s_{r,\mathrm{IF}} \\ \Delta\phi^s_{r,\mathrm{IF}}(i) = d\tilde{t}_r(i) + m^s_r Z_r(i) + \lambda_j \tilde{N}^s_{r,\mathrm{IF}} + \varepsilon^s_{r,\mathrm{IF}} \end{cases} \tag{3}$$

$$\begin{bmatrix} \mathbf{f}^{\mathrm{T}} \cdot (I_2 \otimes \mathbf{c}_p) \cdot \mathbf{f} & \\ & \mathbf{f}^{\mathrm{T}} \cdot (I_2 \otimes \mathbf{c}_\phi) \cdot \mathbf{f} \end{bmatrix} \otimes Q_0 \tag{4}$$

where $\mathbf{f}^{\mathrm{T}} = \begin{bmatrix} f_1^2/(f_1^2 - f_2^2) & -f_2^2/(f_1^2 - f_2^2) \end{bmatrix}$; $\boldsymbol{c}_p$ and $\boldsymbol{c}_\phi$ denote the variance factor matrixes of the pseudorange and carrier phase, respectively; $Q_0 = \mathrm{diag}(1/\sin^2(E_1), 1/\sin^2(E_2), \ldots, 1/\sin^2(E_n))$. Hence, we can express the full-rank design matrix $B$ and estimable parameters $X$ in the IF PPP model with $n$ satellites and the $j$th frequency signal as:

$$B_r(k) = \begin{bmatrix} \begin{pmatrix} m^1_r(k) \\ \cdots \\ m^n_r(k) \end{pmatrix} \otimes e_2 & e_n \otimes e_2 & I_n \otimes \begin{pmatrix} 0 \\ 1 \end{pmatrix} & e_n \otimes \begin{pmatrix} 1 \\ 0 \end{pmatrix} \end{bmatrix} \tag{5}$$

$$X = \begin{bmatrix} Z_r(k) & d\tilde{t}_r(k) & \tilde{N}^1_{r,\mathrm{IF}} \ \ldots \ N^n_{r,\mathrm{IF}} & \tilde{b}_{\mathrm{IF}}(k) \end{bmatrix} \tag{6}$$

with

$$\left.\begin{array}{c} d\tilde{t}_r(i) = dt_r(i) + b_{\mathrm{IF}}(1) \\ \lambda_{\mathrm{IF}}\tilde{N}^s_{r,\mathrm{IF}} = \lambda_{\mathrm{IF}} N^s_{r,\mathrm{IF}} - b^s_{\mathrm{IF}} - b_{\mathrm{IF}}(1) \\ \tilde{b}_{\mathrm{IF}}(i) = b_{\mathrm{IF}}(i) - b_{\mathrm{IF}}(1) \end{array}\right\} \text{when } k \geq 1 \tag{7}$$

where $e_n$ denotes the $n$-row vector wherein all values are 1, $I_n$ denotes the $n$-dimensional identity matrix. $\otimes$ denotes the Kronecker product operation. Identifiers with $\sim$ denote the re-parameterized parameters. However, there will be a rank deficiency between the parameters $dt_r(k)$, $b_{r,\mathrm{IF}}(k)$, and $\lambda_j N^s_{r,\mathrm{IF}}$. For the purpose of eliminating the rank deficiency and enhancing the model, we set the RCBs $b^s_{\mathrm{IF}}(1)$ as a datum. Thus the estimated $\tilde{b}_{\mathrm{IF}}(i)$ values are the variations of RCBs with respect to the first epoch at the first frequency (see equation (7)).

### 2.3. UC PPP model

We only corrected the SCBs in the code observations of the DCB products provided by CAS, and the re-parameterized ambiguities absorbed the code biases in phase observation. As satellite-specific pseudorange biases were eliminated, which implied that the RCB is allowed to freely vary over time, the UC PPP model can be derived as:

$$\begin{cases} \Delta p^s_{r,1}(i) = dt_r(i) + m^s_r T^s_r(i) + \mu_1 I^s_r(i) + b_{r,1}(i) + e^s_{r,1} \\ \Delta p^s_{r,2}(i) = dt_r(i) + m^s_r T^s_r(i) + \mu_2 I^s_r(i) + b_{r,2}(i) + e^s_{r,2} \\ \Delta\phi^s_{r,1}(i) = dt_r(i) + m^s_r T^s_r(i) - \mu_1 I^s_r(i) + \lambda_1 N^s_{r,1} + \varepsilon^s_{r,1} \\ \Delta\phi^s_{r,2}(i) = dt_r(i) + m^s_r T^s_r(i) - \mu_2 I^s_r(i) + \lambda_2 N^s_{r,2} + \varepsilon^s_{r,2} \end{cases} \tag{8}$$

$$\begin{bmatrix} I_2 \otimes \boldsymbol{c}_p & \\ & I_2 \otimes \boldsymbol{c}_\phi \end{bmatrix} \otimes Q_0 \tag{9}$$

with

$$\left.\begin{array}{c} d\tilde{t}_r(i) = dt_r(i) + b_1(1) \\ \lambda_j N^s_{r,j} = \lambda_j N^s_{r,j} - b^s_{\mathrm{IF}} - b_1(1) \\ \tilde{b}_j(i) = b_j(i) - b_1(1) \end{array}\right\} \text{when } k \geq 1. \tag{10}$$

Similarly, the full-rank design matrix and vital parameters in the UC PPP model are given as:

$$B_r(k) = \left[ \begin{pmatrix} m_r^1(k) \\ \cdots \\ m_r^n(k) \end{pmatrix} \otimes e_4 \quad e_n \otimes e_4 \quad I_n \otimes \begin{pmatrix} \mu_1 \\ -\mu_1 \\ \mu_j \\ -\mu_j \end{pmatrix} \quad I_{2n} \otimes \begin{pmatrix} 0 \\ 1 \end{pmatrix} \quad e_n \otimes \begin{pmatrix} 1 & \\ & 1 \end{pmatrix} \right] \tag{11}$$

$$X = \left[ \begin{array}{cccccc} Z_r(k) & dt_r(k) & I_r^1(k) \ \ldots \ I_r^n(k) & N_{r,1}^1, N_{r,2}^1 \ \ldots \ N_{r,1}^n, N_{r,j}^n & \tilde{b}_1(k), & \tilde{b}_2(k) \end{array} \right]. \tag{12}$$

Notably, receiver code bias $\tilde{b}_1(k)$ is assumed to be a time-variant parameter instead of a time-constant one. Through re-parameterization, the rank deficiencies were overcome, resulting in a full-rank functional model, wherein the variations of RCBs on both frequencies between epochs are estimated directly, and thus have no impact on the performance. In the UC PPP model, the temporal variations of the RCBs become estimable and their adverse impacts on PPP parameters, such as ambiguity parameters, receiver clock offsets, and ionospheric delays, are mitigated.

### 2.4. Comparison between the IF PPP and UC PPP models

As described above, the UC PPP and IF PPP functional models are full-rank systems, which facilitate the direct measurement of the temporal variability of RCBs. However, there are apparent differences between the form of estimated receiver biases. The difference between the expressions is the effects of different ionosphere strategies on code bias estimation. Firstly, The UC PPP model provides RCBs for each observable type and observable frequency, thereby making it more flexible. Owing to the low noise of raw observables, the sequence can be predicted to show more variation details. However, the IF PPP model is more robust because of the fewer parameters to be estimated, thereby providing an opportunity to study the influence of RCBs on ambiguity estimates. Moreover, there are obvious differences in the ionospheric processing methods between the two models. Thus, we studied the impact of the ionospheric parameter in the model on the code bias estimation. In the next section, we analyze and compare the results of the two models described in the experimental part and use the RCBs from IF model to verify. Additionally, we use the forward and reverse filtering algorithms to ensure the consistency of the estimation accuracy.

## 3. Data collection and settings

This section starts by detailing the dataset used in the experiment along with the processing strategies, then proceeds with the results and analysis, and ends with some concluding remarks.

As of August 2020, the multi-GNSS experiment (MGEX) and IGS offered a global network of approximately 300 stations of GNSS receivers capable of receiving multi-GNSS and multi-frequency signals. Most of these stations are equipped with Septentrio (30%), Trimble (27%), and Javad (23%) receivers, which are listed in igs20P2116.snx. However, only a few stations are equipped with other receiver types, such as Leica and TPS (<14%) receivers, providing dual-frequency observations. Therefore, we conducted this study with Trimble, Septentrio and Javad receivers, which account for more than 80% of the receivers used in the IGS network.

To achieve global coverage of GNSS stations and to analyze the characteristics of RCBs related to different receiver types, data from 165 globally distributed reference stations archived by the IGS during a period of 7 d in August 2020 were used in this experiment. The 58 and 59 stations equipped with Trimble and Septentrio receivers along with 48 station equipped with Javad receivers, respectively, were selected in our study. These one-week datasets are adequate and beneficial to analyze the intra-day difference of receiver-specific code biases and explore the relationship between RCBs, receiver types, and antenna configuration. Moreover, the observations from the day of year (DOY) 214–220, 2020, with sampling intervals of 30 s, are used in the experiments. The distributions of stations are shown in figure 1.

The precise coordinates of MGEX stations were fixed with the SINEX weekly solutions. In general, the reference coordinates have an accuracy of a few millimeters. The common processing strategies for PPP are summarized in table 1. The initial stochastic model and state update strategies for PPP are presented in table 2, in which $dT$ (s) denotes the interval between epoch $i$ and epoch $i + 1$.

## 4. Results

There is three-part included in this section. We discussed the temporal variation characteristics, inter-day stability, and inter-station correlation of RCB in detail and presented some concluding remarks at last.

### 4.1. The temporal variations of the receiver pseudorange biases

Following the description of the estimation methodology of the two code biases, we derived the daily code biases of four stations at L1 and L2 frequencies with global positioning system (GPS) observables. In the interest of brevity, 'UC' and

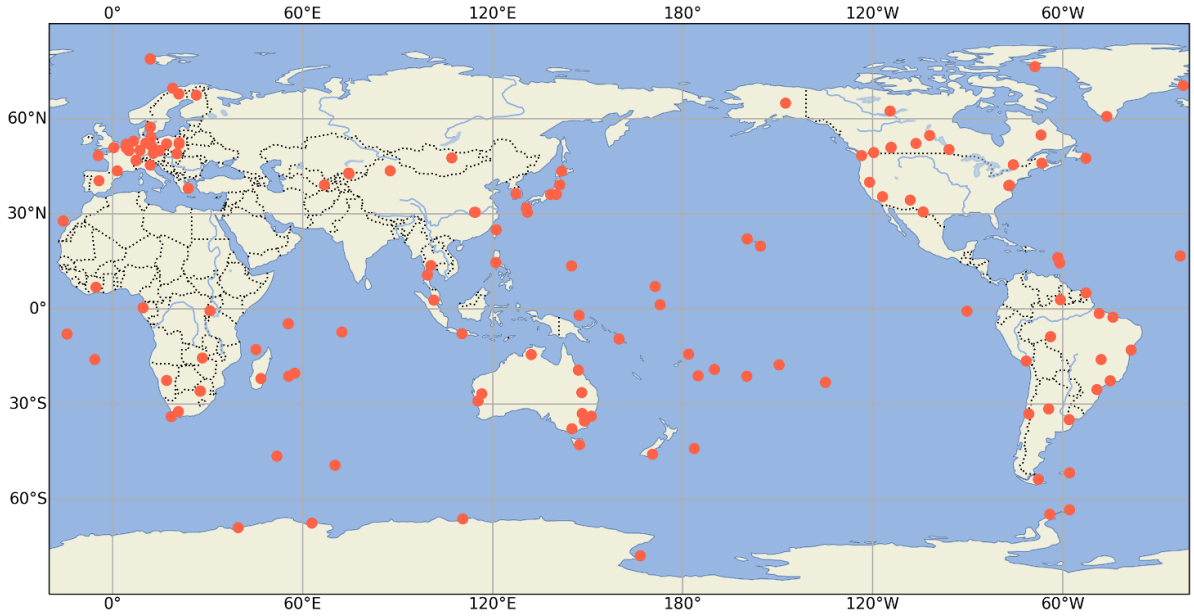


**Figure 1.** The distributions of stations selected for RCB analysis.

**Table 1.** Processing strategies for RCB estimation.

| Items | Model |
|---|---|
| Estimator | Kalman filter |
| Observations | Code and carrier phase measurements (L1/L2), global positioning system (GPS)-only |
| Sampling rate | 30 s |
| Elevation cutoff | 10° |
| Orbit and clock | WUM product [41] |
| DCB correction | CAS MGEX product [42] |
| Weighting scheme | Elevation-dependent; 3 mm and 0.3 m for raw phase and code, respectively |
| Ionospheric delay | IF model: eliminated; UC model: estimated |
| Tropospheric delay | Dry component: corrected with global pressure and temperature model wet component: estimated as a random-walk process, geophysical model mapping function |
| Relativistic effect | Applied |
| Station displacement | Corrected by International Earth Rotation Service Convention 2010, including Solid Earth tide and ocean tide loading |
| Satellite antenna PCO | Corrected with conventional PCO values from MGEX |
| Receiver antenna PCO | Corrected by the same PCO values |
| Phase-windup effect | Corrected |
| Receiver clock | Estimated, epoch-wise solution |
| Station coordinate | Fixed with weekly solution from igs20P2116.snx |
| Phase ambiguities | Estimated, constant for each arc; a float value |

**Table 2.** The stochastic model for RCBs estimation.

| Parameter | Initial variances ($m^2$) | State update ($m^2$) |
|---|---|---|
| Station coordinate | $10 \times 10^{-8}$ | Fixed with $10 \times 10^{-8}$ |
| Ionospheric delay | UC: $5^2$ IF: eliminated | UC: $\sigma_{I_r^s}(i+1) = 0.01^2 \times dT + \sigma_{I_r^s}(i)$ |
| Tropospheric delay | $0.3^2$ | $\sigma_{Z_r}(i+1) = 5.0 \times 10^{-4} \times \sqrt{dT} + \sigma_{Z_r}(i)$ |
| Receiver code biases (RCBs) | $10^2$ | $\sigma_{b_{r,j}}(i+1) = 0.1^2 \times dT + \sigma_{b_{r,j}}(i)$ |
| Receiver clock | $100^2$ | $\sigma_{dt_r}(i+1) = 10^2 + \sigma_{dt_r}(i)$ |
| Phase ambiguities | $100^2$ | $\sigma_{N_{r,j}^s}(i+1) = 0.001^2 \times dT + \sigma_{N_{r,j}^s}(i)$ |

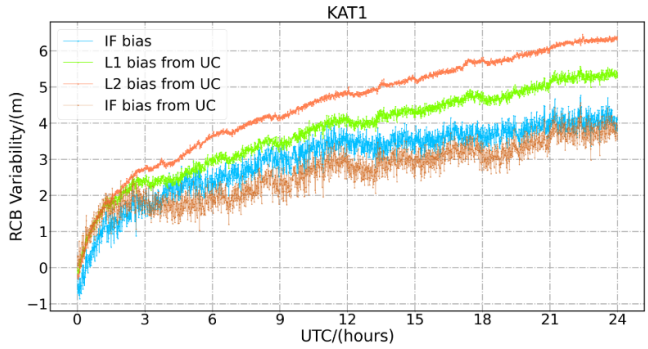


(a) KAT1

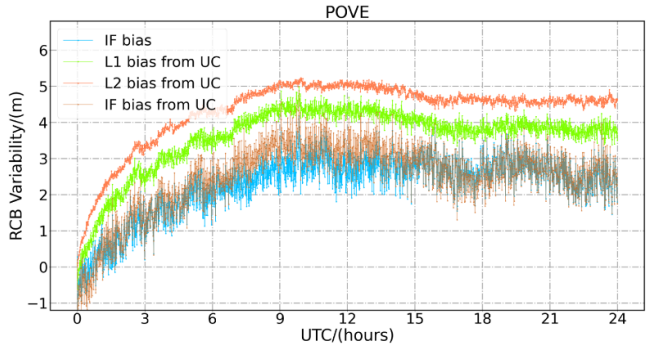


(b) POVE

**Figure 2.** Variation of L1 with time (sky blue lines) and L2 (chartreuse lines) RCBs of KAT1 (upper column) and POVE (lower column) on day 215 in 2020, respectively, as estimated by UC observables and their IF combinations (coral color). The chocolate colored lines depict IF biases with the IF model.

'IF' are used to denote the aforementioned different schemes. Notably, the biases of each frequency are obtained with the UC model, and the biases in the form of IF can be obtained through formula. However, there is a benchmark difference between this deviation and that obtained by the IF model, and a direct comparison cannot be made.

Figure 2 depicts the epoch-by-epoch estimates of RCBs derived by the IF and UC models. As discussed in the section 2, the UC model can derive the pseudorange biases of each independent frequency, while the IF model can only obtain the IF form of RCBs. Compared with the code biases of L1 frequency, the biases on L2 vary more vigorously, but the estimation accuracy is higher. The noise of the L2 observable is smaller, and its precision is slightly better than that of L1 observables, which is proved by Hou *et al* who used Septentrio POLARX4 and Trimble NETR9 receivers [43]. The standard deviation (STD) of L1 RCBs and L2 RCBs are 0.160 and 0.151 m at POVE station, respectively. Notably, the variation range of L2 code biases of the KAT1 and POVE stations is larger than 5 m, which implies that the RCB can not be ignored or treated as a constant in the single-frequency data processing. The variation range of IF pseudorange biases is about 3 m, which is not as vigorous as that of single frequency pseudorange biases. This shows that the IF combination compensates for the variation of pseudorange biases at L1 and L2 frequencies. The IF form of RCB driven by the IF and UC methods is consistent in terms of the variation range. However, owing to the lack of knowledge regarding the specific environments related to the receivers, a detailed interpretation of abnormal intra-day variations range of RCBs is beyond the scope of this study, and the focus of our research is on the driving factors of the changes in the RCB trend. In the following part, the IF method is used to obtain RCBs to study the correlation between RCBs, receiver types, and antenna types.

### *4.2. Inter-day stability of RCB*

We assessed the short-term stabilities of receiver-related pseudorange biases during DOY 214–220, 2020. To prove that the extracted code biases show daily repetition and maintain the similar behaviors between days, we extracted the RCB sequence and used the sequence of the first day to make a difference with other days to obtain a single differenced (SD) sequence of the remaining 6 d. We subtracted the average value from the sequence to ensure the unity of the reference.

The inter-day stability of the receiver pseudorange biases is analyzed using the proposed method combined with the IF model. Additionally, no upgrade of the receiver equipment [28], including receiver type, antenna type, and firmware version, occurred in the selected station during the study period, and the temperature fluctuations in the internal receiver hardware and its antenna within a week were ignored [24]. In previous studies, these factors may have caused the inter-day fluctuation of RCBs. Thus, the proposed method helps in distinguishing whether the RCBs show remarkable inter-day repeatability. The results are depicted in figures 3 and 4. We calculated the standard deviation (STD) value of the SD sequence and depicted its random characteristics using a histogram. As for the ASCG station equipped with the Trimble NETR9 receiver and TRM59800.00 NONE antenna, the STDs of different days were within 0.41 m, and the SD pseudorange bias distribution between days follows the law of normal distribution, which implies that randomness exists. Additionally, different receiver types showed various stabilities. Similar to ASCG, the KRGG station equipped with TRIMBLE ALLOY and antenna LEIAR25.R4 LEIT also exhibited obvious stability; the STDs of SD code biases were smaller than 0.26 m. The SD values of the receiver code estimates are smaller than 0.5 m in more than 95% of these cases. However, the corresponding performance level for the ASCG station only reached 87%.

A similar phenomenon is also reported in the investigation of RCBs using Septentrio receivers or Javad receivers, as shown in figures 4 and 5. As for station OUS2 equipped with a SEPT ASTERX4 receiver and a SEPCHOKE_B3E6 NONE antenna, the STDs of SD were within 0.26 m, and the percentage of code biases less than 0.5 m reached 99% in the best case. This revealed that the RCBs of OUS2 have good consistency between different days. As for station POL2 equipped with a JAVAD TRE_3 DELTA and a TPSCR.G3 NONE antenna, the STDs of SD were within 0.20 m, and the percentage of code

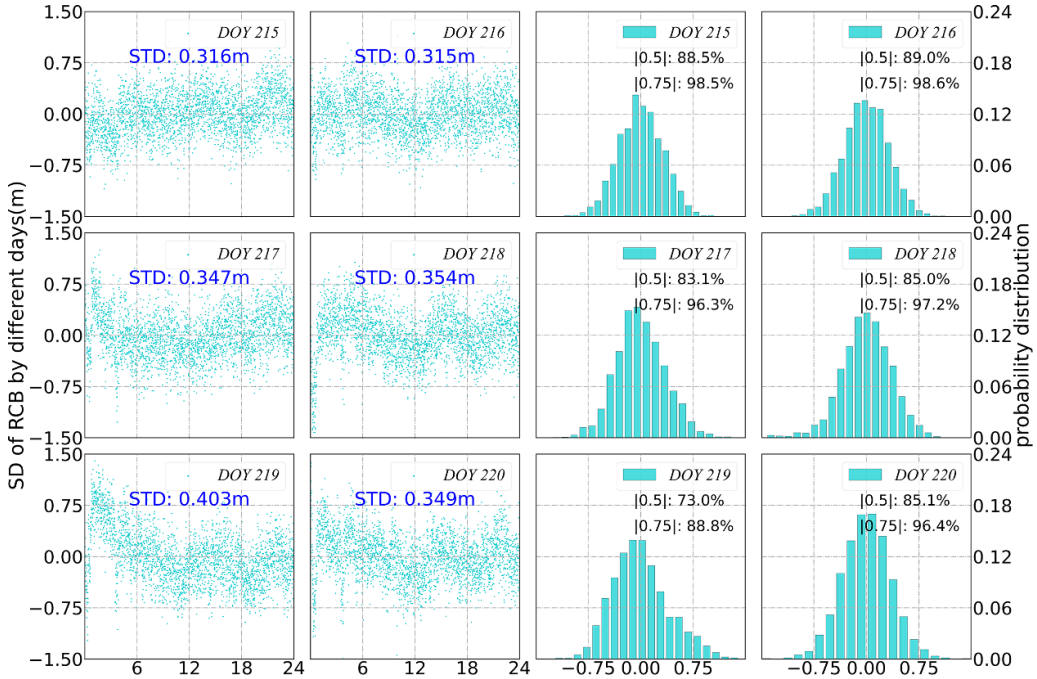


**Figure 3.** The SD series of inter-day RCBs from the ASCG station, with the RCBs from DOY 214 in 2020 as reference (left column). Distribution of the inter-day stability of RCBs estimates from DOY 214–220 in 2020 (right column); the vertical axis represents the percentage, and the horizontal axis represents the SD of the RCBs estimated over a 1 d period. |0.5| and |0.75| represent the percentage of cases wherein the |SD| is smaller than 0.5 and 0.75 m, respectively.

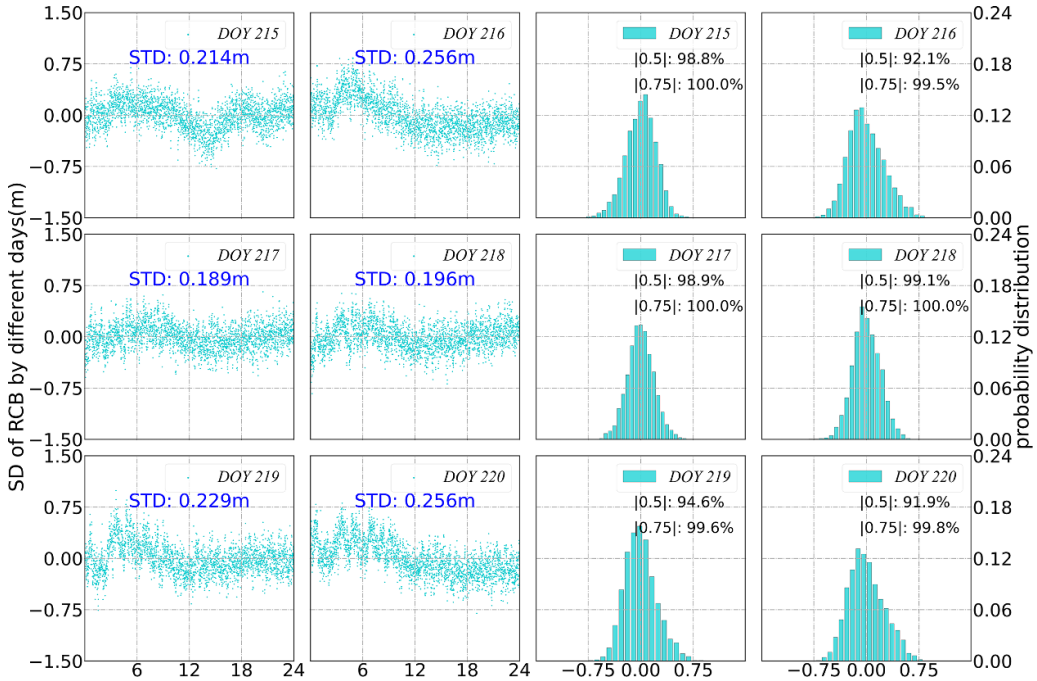


**Figure 4.** The SD series of OUS2 RCB of inter-day with the RCB of DOY 214 as reference (left column). Distribution of the inter-day stability of RCBs estimates for the period of DOY 214–220 in 2020 (right column); the vertical axis represents the percentage, and the horizontal axis represents the SDs of the RCBs estimates over a 1 d period.

biases less than 0.5 m reached 100.0% in the best case. This revealed that the RCBs of POL2 have better stability over consecutive 7 d. Moreover, there is no obvious decline in the consistency of RCBs in the short term. Therefore, we estimated that receiver-related pseudorange biases were quite stable in the short term and show daily repetition characteristics; however, the intra-day variations of receiver pseudorange biases are not stable, as shown in the first part.

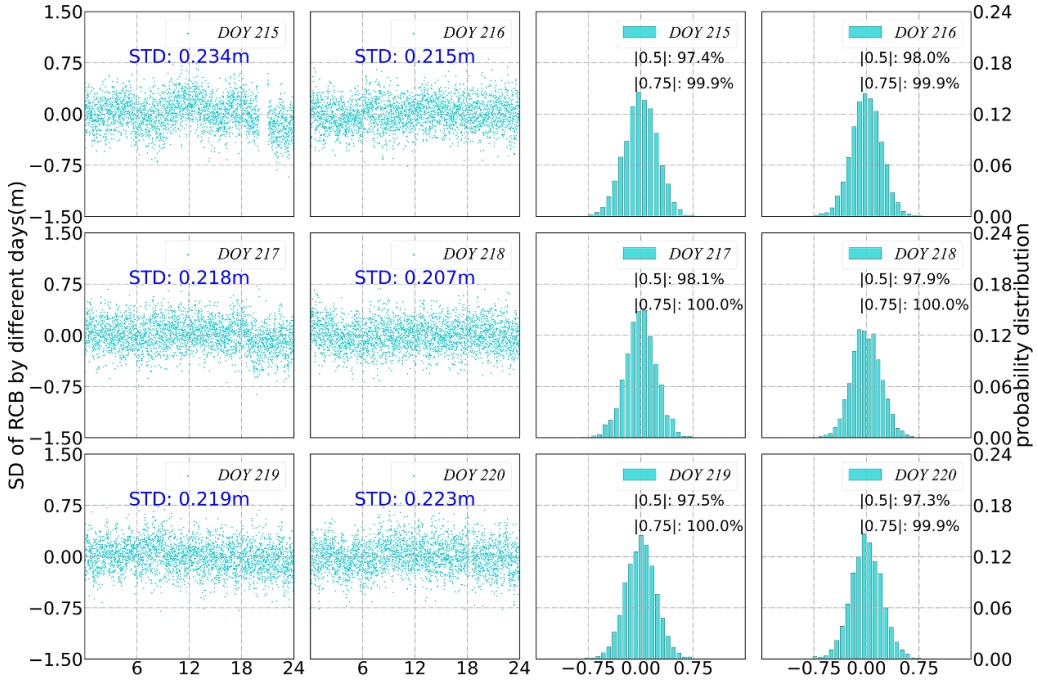


**Figure 5.** The SD series of POL2 RCB of inter-day with the RCB of DOY 214 as reference (left column). Distribution of the inter-day stability of RCBs estimates for the period of DOY 214–220 in 2020 (right column); the vertical axis represents the percentage, and the horizontal axis represents the SDs of the RCBs estimates over a 1 d period.

**Table 3.** Information on the mean SD values from stations equipped with Trimble or SEPT receivers.

| Receiver types | The ratio of SDs mean values in \|0.5 m\| | The ratio of SDs mean values in \|0.75 m\| | STDs of SDs mean values |
|---|---|---|---|
| Trimble | 74.83% | 89.13% | 0.45 m |
| Septentrio | 85.57% | 94.39% | 0.33 m |
| Javad | 84.35% | 94.69% | 0.36 m |

We average the SD values of the receiver code estimates from all selected stations, equipped with both Trimble (58 stations), Septentrio (57 stations) or Javad (48 stations) receivers. For Trimble receivers, the SD is smaller than 0.5 m in more than 74.83% of the cases for all of the receivers (table 3). Alternatively, for Septentrio receivers, the SD values are less than 0.5 m in more than 85.57% of the cases and Javad receivers can reach 84.35%. The mean STDs of SD values are 0.45, 0.33 and 0.36 m for Trimble, Septentrio and Javad receivers, respectively. In general, this shows that significant inter-day fluctuations have not occurred in almost all stations. Meantime, we count the number of stations under different sequences of the probability of SD values between −0.5 and 0.5 m, and between −0.75 and 0.75 m, as presented in tables 4 and 5. Notably, all selected stations show that more than 50% of SD values of the receiver code estimates are smaller than 0.5 m, and more than 70% of the SD values are smaller than 0.75 m for Trimble receivers. Septentrio receivers show higher values of 65% and 75% and Javad receivers have higher values of 70% and 80%. Moreover, under strict conditions (more than 95% of SD values of the receiver code estimates are smaller than 0.75 m), 20, 36 and 31 stations configured with Trimble, Septentrio and Javad receivers still meet the required conditions. Nevertheless, we can still conclude that the RCBs of partial receivers existed, and have a significant characteristic of stability. This indicates that the code biases may be calibrated by external products in the SINEX format.

### *4.3. Inter-station correlation of RCBs*

In this part, we analyze the relationship between the inter-station correlation of the code deviation and the receiver and antenna configurations. To determine whether the RCBs of the stations equipped with similar receivers and antennas have similar behavior, we conducted six groups of experiments, three of which included Septentrio receivers, and the other three included Trimble receivers. Table 6 presents the information of the selected GNSS station. These stations are selected from some major GNSS observation networks, such as Geoscience Australia, GSI, ESOC, IBGE, and Swiss Federal Office of Topography, which are managed and maintained by the same official agency. This ensures that the operation and settings of the receiver and antenna are consistent. We used the data of different distances between stations for the analysis, by averaging the RCBs on a daily basis. This could prevent the spatial correlation enhancement caused by short distances as well as incorrect analyses and conclusions.

Firstly, we calculate the between-receiver (BR) RCBs between KAT1 and TOW2 using the UC and IF models. Moreover, we confirm the consistency of the inter-station deviation analysis of the two models, which corresponds to our previous conclusion.

**Table 4.** The number of stations under different sequences of the probability of SD values between −0.5 and 0.5 m.

| The ratio for SDs in \|0.5 m\| | 50% | 60% | 70% | 80% | 90% |
|---|---|---|---|---|---|
| Stations equipped with Trimble | 58 | 51 | 38 | 24 | 5 |
| Stations equipped with Septentrio | 57 | 57 | 51 | 41 | 25 |
| Stations equipped with Javad | 48 | 48 | 48 | 42 | 39 |

**Table 5.** The number of stations under different sequences of probability of SD values between −0.75 and 0.75 m.

| The ratio for SDs in \|0.75 m\| | 70% | 75% | 80% | 85% | 90% | 95% |
|---|---|---|---|---|---|---|
| Stations equipped with Trimble | 58 | 54 | 49 | 39 | 31 | 20 |
| Stations equipped with Septentrio | 57 | 57 | 55 | 51 | 45 | 36 |
| Stations equipped with Javad | 48 | 48 | 48 | 42 | 39 | 31 |

**Table 6.** The information on the collected GPS data used in this study.

| Scheme | Station | Length | Receiver | Firm. Ver. | Antenna type | Latitude, longitude |
|---|---|---|---|---|---|---|
| A | KAT1 | 1,672 km | SEPT POLARX5 | 5.3.2 | LEIAR25. R3 LEIT | 14.376° S, 132.153° E |
| | TOW2 | | SEPT POLARX5 | 5.3.2 | LEIAR25.R3. NONE | 19.269° S, 147.056° E |
| B | PADO | Max: 381 km | SEPT POLARX5 | 5.3.2 | SEPCHOKE_B3E6 SPKE | 45.411° N, 11.896° E |
| | REDU | Min: 718 km | SEPT POLARX5 | 5.3.2 | SEPCHOKE_B3E6 NONE | 50.001° N, 5.144° E |
| | WAB2 | | SEPT POLARX5TR | 5.3.2 | SEPCHOKE_B3E6 SPKE | 46.924° N, 7.464° E |
| C | YAR3 | 20.21 m | SEPT POLARX5 | 5.3.2 | LEIAR25 NONE | 29.046° S, 115.347° E |
| | YARR | | SEPT POLARX5 | 5.3.2 | LEIAT504 NONE | 29.046° S, 115.347° E |
| D | BELE | 1,884 km | TRIMBLE NETR9 | 5.45 | TRM115000.00. NONE | 1.409° S, 48.462° W |
| | POVE | | TRIMBLE NETR9 | 5.45 | TRM115000.00. NONE | 8.709° S, 63.896° W |
| E | ISHI | 16.49 km | TRIMBLE NETR9 | 5.45 | TRM59800.00 SCIS | 36.208° N, 140.218° E |
| | TSK2 | | TRIMBLE NETR9 | 5.45 | TRM59800.00 NONE | 36.106° N, 140.087° E |
| F | ZIM2 | Max: 18.71 m | TRIMBLE NETR9 | 5.45 | TRM59800.00 NONE | 46.877° N, 7.465° E |
| | ZIM3 | | TRIMBLE NETR9 | 5.45 | TRM59800.00 NONE | |
| | ZIMM | | TRIMBLE NETR9 | 5.45 | TRM29659.00 NONE | |

For example, as shown in figure 6, the root mean square (RMS) of the code biases estimated by the IF model is approximately 0.7 m, while that of biases estimated by the UC model is approximately 0.6 m. As for BELE-POVE, the stations in scheme D were all equipped TRIMBLE receivers, and the RMS values of BR RCBs using the UC and IF models are 0.65 and 0.67 m, respectively. For schemes A and D, the distance between the two stations is more than 1000 km and there is almost no spatial correlation. The RCBs of the two stations still maintain considerable variation trends, especially in KAT1-TOW2.

Subsequently, we discuss and analyze the possible correlation between the RCBs and the receiver and antenna hardware. We obtained a difference between the RCBs of different stations, and the acquired result is termed as BR-RCBs. We calculated the RMS and STD values of BR-RCBs under different cases in the next step. The Pearson correlation coefficient (PCC) is adopted to assess the correlation of the short-term variability of RCBs between different stations. The statistical result of BR-RCBs under different configurations are presented in table 7.

As for KAT1-TOW2, the station is completely equipped with SEPT POLARX5 receivers, and the receiver firmware version is the same. The type of antenna is LEIAR25. R3 and radome types are slightly different. The radome type can capture free electromagnetic signals from a distorted setting or after attenuation under bad weather conditions. The PCC value between the RCBs of KAT1 and TOW2 is higher than 0.91, indicating that RCBs between KAT1 and TOW2 have similar performances. Notably, the STD value of BR-DCB is smaller than half of the RMS value. When we subtract the existing reference difference from BR-DCB, the BR-DCB value shows noise characteristics. All statistical results confirm a notable positive correlation between the RCBs of KAT1 and TOW2.

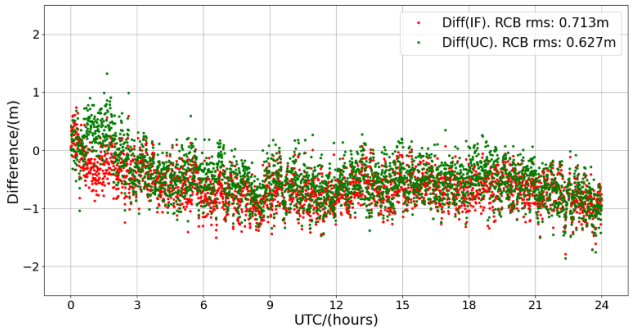


(a) KAT1-TOW2

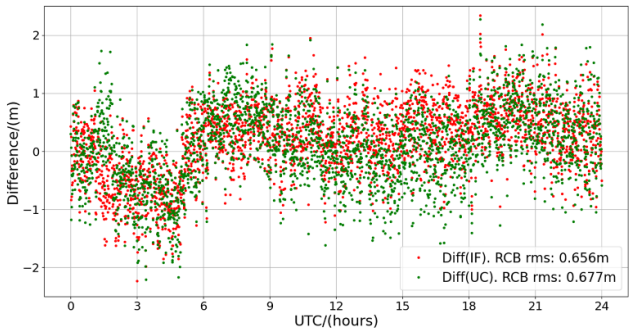


(b) BELE-POVE

**Figure 6.** BR RCBs of KAT1-TOW2 (a) and BELE-POVE (b) on DOY 215 in 2020, respectively, as estimated by UC observables (red). The green point depicts the BR RCB estimated using the IF model.

**Table 7.** The statistical result of BR-RCBs with six groups of configurations.

| Case | Scheme | STD (m) | RMS (m) | PCC | Length |
|---|---|---|---|---|---|
| KAT1-TOW2 | A | 0.327 | 0.713 | 0.953 | 1672 km |
| PADO-REDU | B | 0.246 | 0.572 | 0.924 | 718 km |
| PADO-WAB2 | | 0.198 | 0.336 | 0.951 | 381 km |
| REDU-WAB2 | | 0.246 | 0.825 | 0.927 | 382 km |
| YAR3-YARR | C | 0.172 | 0.718 | 0.971 | 20.21 m |
| BELE-POVE | D | 0.630 | 0.656 | 0.679 | 1884 km |
| ISHI-TSK2 | E | 0.303 | 0.306 | 0.602 | 16.49 km |
| ZIM2-ZIM3 | F | 0.236 | 0.265 | 0.923 | 0 m |
| ZIM2-ZIMM | | 0.320 | 0.420 | 0.668 | 18 m |
| ZIM3-ZIMM | | 0.403 | 0.563 | 0.692 | 18 m |

There are three stations in scheme B; two of them are equipped with SEPT POLARX5 receivers, and the other is equipped with a SEPT POLARX5TR receiver. The antennas connected are SEPCHOKE_B3E6. Figure 7 shows the BR-RCB in (a) PADO-REDU, (b) PADO-WAB2, and (c) REDU-WAB2. We found that the correlation between stations will not be affected by the distance when it exceeds hundreds of kilometers. The PCCs in scheme B are higher than 0.9, which is a significant index in correlation analysis. Notably, the correlation of RCBs between PADO and WAB2 is more obvious, which is hard to explain considering the lack of relevant hardware knowledge. Nevertheless, we still confirm the existence of partial receivers showing significant consistency in the intra-day variation of RCBs. A similar phenomenon also appears in BR-RCBs between YAR3 and YARR in scheme C. A better result can be found in this case. It is possible that a similar spatial effect due to short distance has enhanced the correlation of code biases.

Compared with that of Septentrio receivers, this inter-station relationship of RCBs is not significant among Trimble receivers. We also chose three sets of data from long to short for analysis. The STD values of BR-DCB are not notably reduced after subtracting the reference difference. However, a relationship still exists between the RCBs and the antenna

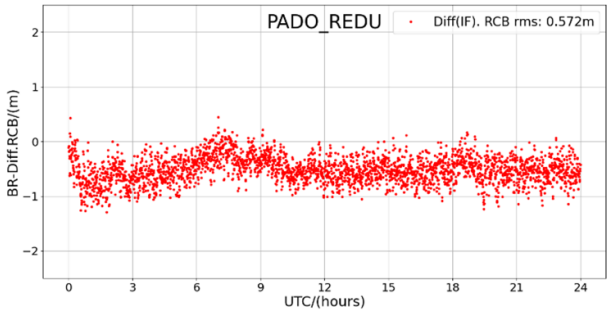


(a) PADO-REDU

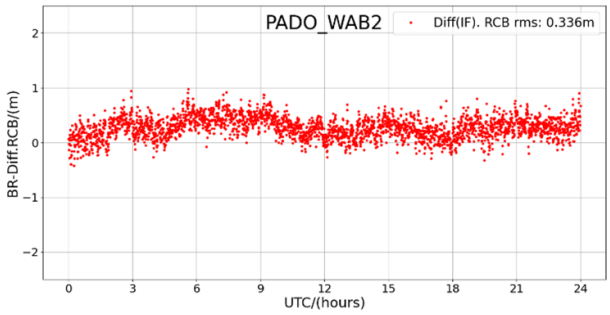


(b) PADO-WAB2

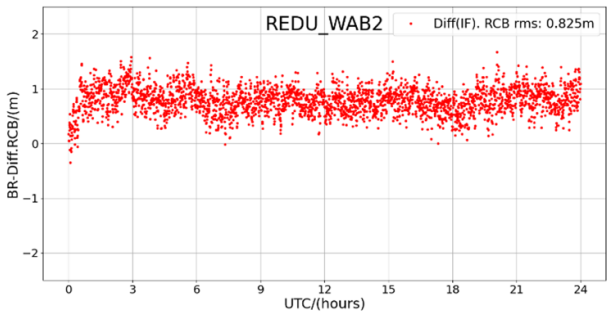


(c) REDU-WAB2

**Figure 7.** BR RCBs of (a) PADO-REDU, (b) PADO-WAB2, and (c) REDU-WAB2 on DOY 217 in 2020, respectively.

type, especially in scheme F. As the receiver was connected to the antenna of the same type, the RCBs between ZIM2 and ZIM3 have a strong similarity and the PCC is 0.923. Figure 8 shows BR-RCBs of ZIM2-ZIM3 on DOY 215 of 2020. The STD of BR-RCB is close to the RMS, which illustrates that the reference difference is similar and may be caused by the zero baseline setup. When we compare ZIM2 and ZIMM, the correlation of RCB drops significantly for different antenna configurations, although the distance is short. Moreover, a similar spatial effect result in the STD value is similar to the RMS. This confirms that the receiver pseudorange biases are affected by the receiver and antenna setup. When dealing with GNSS network data provided by inhomogeneous receivers, receiver-related pseudorange biases will lead to the loss of precision or result in the potential correlation between observables.

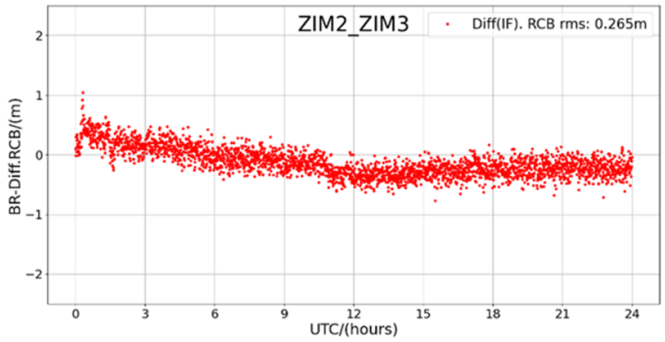


**Figure 8.** BR RCBs of ZIM2-ZIM3 on DOY 215 in 2020, respectively. The stations ZIM2 and ZIM3 represent zero-baseline setup and are equipped with the TRIMBLE NETR9 receiver connected to the same antenna.

## 5. Conclusions

Although receiver-related pseudorange biases are known to be caused by the different designs of receiver front ends, correlator spacing, and multipath mitigation techniques adopted in receivers, there is a lack of investigation on the consistency of the RCB variations between receivers. Additionally, estimating the code biases is challenging in their undifferenced form because they are lumped into the receiver with clock offsets. Based on the analysis concerning the RCBs, some conclusions can be drawn.

In this study, we presented the detailed research of GPS receiver-related pseudorange biases with the Septentrio and Trimble receivers in the IGS network. We have raised two PPP models, the IF and UC models, respectively, to extract the time-varying pseudorange biases for each receiver. Firstly, we compared the IF and UC models and found that they can both be used for RCB estimation. The IF biases are obtained without the impact of the ionosphere, while the biases in each frequency are estimated. The variation of IF pseudorange biases is about 3 m, which is not as extensive as that of pseudorange biases on a single frequency.

Secondly, we assessed the inter-day stability of RCBs with weekly observations of 165 stations with three types of receivers. The results indicated that there was significant stability of receiver-related pseudorange biases in the short term. As for station OUS2, the STDs of SD were within 0.26 m, and the percentage of SD code biases less than 0.5 m reached 99% in the best case. The KRGG station equipped with TRIMBLE ALLOY receivers and a LEIAR25.R4 LEIT antenna also exhibit obvious stability; the STDs of SD code biases are smaller than 0.26 m, and the percentage of SD values smaller than 0.5 m is more than 95%. For the Septentrio receiver, we found that the ratio of stations is 74.83% when that the mean SD values are between −0.5 and 0.5 m. Among Septentrio receivers, 85.57% of the stations show SD values between −0.5 and 0.5 m. We also found that the ratio of stations that equipped with Javad receiver can reach 84.35% when that the mean SD

values are between −0.5 and 0.5 m. We concluded that the time series of receiver related pseudorange biases proved that these biases were stable over the consecutive days in a week from the view of short-term variation trends.

Thirdly, we also studied the relationship between receiver-related pseudorange biases and the receiver and antenna type. We conducted six sets of comparative experiments involving 14 stations. The relationship between RCBs and antenna type is more obvious among Septentrio receivers. The PCCs are all higher than 0.9 in schemes equipped with Septentrio receivers, which is a significant index in correlation analysis. Notably, there is a strong relationship between receiver-related pseudorange biases and the receiver and antenna setup.

In the future, GNSS receiver-related pseudorange biases may be calibrated for each receiver and antenna combination type with an external model or OSB products in the SINEX format. Moreover, the RCBs have still not been studied enough, and more studies are required to understand them further. It is noted that the RCBs should also be considered in the PPP functional model as time-variant parameters.

## Data availability statements

The observation, navigation, antenna information, and weekly solution in the SINEX format were obtained from CDDIS: https://cddis.gsfc.nasa.gov. The final precise multi-GNSS satellite orbit and clock products provided by the GNSS Research Center of Wuhan University are available at https://igs.gnsswhu.cn/pub/gnss/products/mgex. The DCB products are provided by CAS at https://gipp.org.cn/product/dcb/mgex/2020. The detailed site information of IGS stations is provided by IGS FTP server at https://files.igs.org/pub/station/log/.

The data that support the findings of this study are available upon reasonable request from the authors.

## Acknowledgments

We offer many thanks to the IGS MGEX, Wuhan University, and CAS for providing access to multi-GNSS data and DCB products. We thank three anonymous reviewers for their insightful comments and suggestions to improve our manuscript.

## Fundings

This research was jointly funded by the National Key Research Program of China: ‘Collaborative Precision Positioning Project’ (No. 2016YFB0501900) and the National Natural Science Foundation of China (No. 42074045).

## ORCID iD

Luohong Li https://orcid.org/0000-0003-0308-0977

## References

[1] Håkansson M, Jensen A B O, Horemuz M and Hedling G 2017 Review of code and phase biases in multi-GNSS positioning *GPS Solut.* **21** 849–60
[2] Wang Y, Zhao L and Gao Y 2020 Determination and analysis of front-end and correlator-spacing-induced biases for code and carrier phase observations *Meas. Sci. Technol.* **31** 115011
[3] Zhang Y, Kubo N, Chen J and Wang A 2021 Calibration and analysis of BDS receiver-dependent code biases *J. Geod.* **95** 43
[4] Lou Y, Gong X, Gu S, Zheng F and Feng Y 2017 Assessment of code bias variations of BDS triple-frequency signals and their impacts on ambiguity resolution for long baselines *GPS Solut.* **21** 177–86
[5] Chuang S, Wenting Y, Weiwei S, Yidong L, Yibin Y and Rui Z 2013 GLONASS pseudorange inter-channel biases and their effects on combined GPS/GLONASS precise point positioning *GPS Solut.* **17** 439–51
[6] Gu S, Wang Y T, Zhao Q, Zheng F and Gong X 2020 BDS-3 differential code bias estimation with undifferenced uncombined model based on triple-frequency observation *J. Geod.* **94** 45
[7] Mi X, Zhang B, Yuan Y and Luo X 2020 Characteristics of GPS, BDS2, BDS3 and Galileo inter-system biases and their influence on RTK positioning *Meas. Sci. Technol.* **31** 015009
[8] Zhang B and Teunissen P J G 2016 Zero-baseline analysis of GPS/BeiDou/Galileo between-receiver differential code biases (BR-DCBs): time-wise retrieval and preliminary characterization *Navig. J. Inst. Navig.* **63** 181–91
[9] Zhang X, He X and Liu W 2017 Characteristics of systematic errors in the BDS Hatch–Melbourne–Wübbena combination and its influence on wide-lane ambiguity resolution *GPS Solut.* **21** 265–77
[10] Li M, Yuan Y, Wang N, Li Z, Li Y and Huo X 2017 Estimation and analysis of Galileo differential code biases *J. Geod.* **91** 279–93
[11] Schaer S 2016 SINEX BIAS—solution (software/technique) INdependent EXchange format for GNSS BIASes version 1.00 vol 2015 pp 5–6 (available at: https://files.igs.org/pub/data/format/sinex_bias_100.pdf)
[12] Villiger A, Schaer S, Dach R, Prange L, Sušnik A and Jäggi A 2019 Determination of GNSS pseudo-absolute code biases and their long-term combination *J. Geod.* **93** 1487–500
[13] Li W, Li M, Shi C, Fang R, Zhao Q, Meng X, Yang G and Bai W 2017 GPS and BeiDou differential code bias estimation using Fengyun-3C satellite onboard GNSS observations *Remote Sens.* **9** 1239
[14] Liu T, Yuan Y, Zhang B, Wang N, Tan B and Chen Y 2017 Multi-GNSS precise point positioning (MGPPP) using raw observations *J. Geod.* **91** 253–68
[15] Khodabandeh A and Teunissen P J G 2016 PPP-RTK and inter-system biases: the ISB look-up table as a means to support multi-system PPP-RTK *J. Geod.* **90** 837–51
[16] Jiang N, Xu Y, Xu T, Xu G, Sun Z and Schuh H 2017 GPS/BDS short-term ISB modelling and prediction *GPS Solut.* **21** 163–75
[17] Wanninger L and Beer S 2015 BeiDou satellite-induced code pseudorange variations: diagnosis and therapy *GPS Solut.* **19** 639–48
[18] Gong X, Gu S, Zheng F, Wu Q, Liu S and Lou Y 2021 Improving GPS and Galileo precise data processing based on calibration of signal distortion biases *Measurement* **174** 108981
[19] Zheng F, Gong X, Lou Y, Gu S, Jing G and Shi C 2019 Calibration of BeiDou triple-frequency receiver-related

pseudorange biases and their application in BDS precise positioning and ambiguity resolution *Sensors* **19** 3500
[20] Li M, Yuan Y, Wang N, Liu T and Chen Y 2018 Estimation and analysis of the short-term variations of multi-GNSS receiver differential code biases using global ionosphere maps *J. Geod.* **92** 889–903
[21] Cui B, Li P, Wang J, Ge M and Schuh H 2021 Calibrating receiver-type-dependent wide-lane uncalibrated phase delay biases for PPP integer ambiguity resolution *J. Geod.* **95** 82
[22] He C, Lu X, Guo J, Su C, Wang W and Wang M 2020 Initial analysis for characterizing and mitigating the pseudorange biases of BeiDou navigation satellite system *Satell. Navig.* **1** 3
[23] Liu S and Yuan Y 2021 A method to accelerate the convergence of satellite clock offset estimation considering the time-varying code biases *Remote Sens.* **13** 2714
[24] Cheng L, Wang W, Liu J, Lv Y and Geng T 2021 GNSS receiver-related pseudorange biases: characteristics and effects on wide-lane ambiguity resolution *Remote Sens.* **13** 428
[25] Rovira-Garcia A, Juan J M, Sanz J and Gonzalez-Casado G 2015 A worldwide ionospheric model for fast precise point positioning *IEEE Trans. Geosci. Remote Sens.* **53** 4596–604
[26] Yuan Y, Zhang K, Rohm W, Choy S, Norman R and Wang C 2014 Real-time retrieval of precipitable water vapor from GPS precise point positioning *J. Geophys. Res. Atmos.* **119** 10044–57
[27] Ge Y, Zhou F, Liu T, Qin W J, Wang S and Yang X 2019 Enhancing real-time precise point positioning time and frequency transfer with receiver clock modeling *GPS Solut.* **23** 20
[28] Zhang B, Teunissen P J G, Yuan Y, Zhang H and Li M 2018 Joint estimation of vertical total electron content (VTEC) and satellite differential code biases (SDCBs) using low-cost receivers *J. Geod.* **92** 401–13
[29] Banville S and Langley R B 2011 Defining the basis of an 'integer-levelling' procedure for estimating slant total electron content *24th Int. Technical Meeting of the Satellite Division of the Institute of Navigation 2011, ION GNSS 2011* vol 4 pp 2542–51
[30] Coster A, Williams J, Weatherwax A, Rideout W and Herne D 2013 Accuracy of GPS total electron content: GPS receiver bias temperature dependence *Radio Sci.* **48** 190–6
[31] Wanninger L, Sumaya H and Beer S 2017 Group delay variations of GPS transmitting and receiving antennas *J. Geod.* **91** 1099–116
[32] Wanninger L 2012 Carrier-phase inter-frequency biases of GLONASS receivers *J. Geod.* **86** 139–48
[33] Xue J, Song S and Zhu W 2016 Estimation of differential code biases for BeiDou navigation system using multi-GNSS observations: how stable are the differential satellite and receiver code biases? *J. Geod.* **90** 309–21
[34] Zha J, Zhang B, Yuan Y, Zhang X and Li M 2019 Use of modified carrier-to-code leveling to analyze temperature dependence of multi-GNSS receiver DCB and to retrieve ionospheric TEC *GPS Solut.* **23** 103
[35] Zhang B, Teunissen P J G and Yuan Y 2017 On the short-term temporal variations of GNSS receiver differential phase biases *J. Geod.* **91** 563–72
[36] Zhang B, Zhao C, Odolinski R and Liu T 2021 Functional model modification of precise point positioning considering the time-varying code biases of a receiver *Satell. Navig.* **2** 11
[37] O'Brien A J and Gupta I J 2011 Mitigation of adaptive antenna induced bias errors in GNSS receivers *IEEE Trans. Aerosp. Electron. Syst.* **47** 524–38
[38] Pan L, Zhang X and Liu J 2019 A comparison of three widely used GPS triple-frequency precise point positioning models *GPS Solut.* **23** 121
[39] Leick A, Rapoport L and Tatarnikov D 2015 *GPS Satellite Surveying* (New York: Wiley)
[40] Sterle O, Stopar B and Pavlovčič Prešeren P 2015 Single-frequency precise point positioning: an analytical approach *J. Geod.* **89** 793–810
[41] Guo J, Xu X, Zhao Q and Liu J 2016 Precise orbit determination for quad-constellation satellites at Wuhan University: strategy, result validation, and comparison *J. Geod.* **90** 143–59
[42] Wang N, Yuan Y, Li Z, Montenbruck O and Tan B 2016 Determination of differential code biases with multi-GNSS observations *J. Geod.* **90** 209–28
[43] Hou P, Zhang B and Yuan Y 2021 Analysis of the stochastic characteristics of GPS/BDS/Galileo multi-frequency observables with different types of receivers *J. Spat. Sci.* **66** 49–73